Subsurface Sediment Mobilization in the Southern Chryse Planitia on Mars

P. Brož[1*], E. Hauber[2], I. van de Burgt[2], V. Špillar[3], G. Michael[4]

[1]Institute of Geophysics of the Czech Academy of Science, Boční II/1401, 141 31, Prague, Czech Republic

[2]Institute of Planetary Research, DLR, Rutherfordstr. 2, 12489, Berlin, Germany

[3]Charles University in Prague, Faculty of Science, Institute of Petrology and Structural Geology, Albertov 6, 128 00, Prague, Czech Republic

[4] Freie Universität Berlin, Malteser Strasse 74-100, Berlin 12249, Germany

Corresponding Author

Petr Brož

Institute of Geophysics of Czech Academy of Science (CAS) v.v.i

Boční II/1401

14131 Prague 4

Czech Republic

Petr.broz@ig.cas.cz

+420267103063

Key points

- Southern Chryse Planitia contains a large field of Amazonian-aged extrusive landforms which can be grouped into five classes.
- They are exclusively located in the sedimentary plains between erosional remnants suggesting that they were formed by sedimentary volcanism.
- The variability in shapes can be explained by properties of the mud and environment.

Abstract

The southern part of the smooth plain of Chryse Planitia on Mars hosts a large population of kilometer-sized (from ~0.2 to ~20 km) landforms spread over a wide area. Based on the investigation of a small part of this area, Komatsu and co-workers [2016; http://dx.doi.org/10.1016/j.icarus.2015.12.032] proposed that the edifices may be the result of the subsurface sediment mobilization. We mapped the full extent of these landforms within Chryse Planitia and performed a morphological and spatial analysis in an attempt to further test this hypothesis. We identified a total number of 1318 of these objects, which we grouped into five different morphological classes. The edifices can be observed over an area of 700,000 km^2 near the termini of the large outflow channels, Ares, Simud and Tiu Valles, with a non-random spatial distribution. The features are clustered and anticorrelated to the ancient highlands, which form erosional remnants shaped by the outflow events. This suggests a genetic link between the distribution of the edifices and the presence of the sedimentary deposits on which they are superposed. Such distribution is consistent with the previous notion that subsurface sediment mobilization may be the mechanism for their formation and is less consistent with the alternative igneous volcanic hypothesis. We also propose a scenario in which the large morphologic variability can be explained by variations of the water content within the ascending mud, and by variations in the effusion rates. The edifices may represent one of the most prominent fields of sedimentary volcanism detected on Mars.

Plain language summary

Ever since the presence of methane in the Martian atmosphere was reported from ground-based, orbital, and in situ observations, mud volcanism was hypothesized to be a possible release mechanism, and various mud volcano fields have been tentatively identified. Although morphological similarities with Earth sedimentary volcanism have been proposed (e.g. *Skinner and Mazzini*, 2009), it is difficult, however, to prove unambiguously the presence of mud volcanism in remote sensing data, and some of the reported mud volcanoes have alternatively been interpreted as igneous volcanoes. A definitive identification of sedimentary volcanoes on Mars is therefore still problematic. A useful candidate area to test the hypothesis of sedimentary volcanism on Mars is a field of kilometer-sized cone- and pie-like landforms in the southern part of the large ancient Chryse impact basin, part of which was previously studied by *Komatsu* and colleagues [2016]. In this study we searched for those landforms inside Chryse Planitia and determined their full spatial extent. We found that they can be divided into five morphologically different groups and that occur exclusively on the level sedimentary plains. These findings enables us providing additional evidence to support the hypothesis of subsurface sediment mobilization as a possible mechanism for their formation.

1. Introduction

Ever since the presence of methane in the Martian atmosphere was reported from ground-based, orbital, and in situ observations [*Krasnopolsky et al.,* 2004; *Mumma et al.,* 2009; *Formisano et al.*, 2004; *Geminale et al.*, 2011; *Webster et al.*, 2018], mud volcanism was hypothesized to be a possible release mechanism [reviewed by *Oehler and Etiope*, 2017], and various mud volcano fields have been tentatively identified [*Skinner and Tanaka*, 2007; *Skinner and Mazzini*, 2009; *Pondrelli et al*., 2011; *Oehler and Allen*, 2012; *Allen et al*., 2013; *Salvatore and Christensen*, 2015; *Okubo*, 2016; *Komatsu et al*., 2016; *Hemmi and Miyamoto*, 2018]. It is difficult, however, to define diagnostic morphological properties of mud volcanism in remote sensing data [*Oehler and Allen*, 2010], and some of the reported mud volcanoes have alternatively been interpreted as igneous volcanoes [*Brož and Hauber*, 2013; *Brož et al*., 2017]. Moreover, mud volcanism on Earth has the following characteristics, some of which (e.g., presence of hydrocarbon reservoirs) may not be easily encountered on Mars: (1) an origin from thick, rapidly deposited sequences, sometimes associated with gravitational instabilities; (2) a link to tectonic activity, both at active and passive margins; (3) over- or underpressurization of sediments and accompanying fluid emission (gas, brines, gas hydrate water, or hydrocarbons); and (4) eruption of mud breccia at the crater site [*Kopf*, 2002, *Mazzini and Etiope*, 2017]. Given that it remains unknown if these characteristic are/were present in the Martian subsurface, the usage of the term 'mud volcanism' for Martian phenomena may be therefore misleading and consequently, a more general term is used within this text, i.e. subsurface sediment mobilization, a collective term including soft sediment deformations, sand injections, shale diapirs, hydrothermal vent complexes and sediment-hosted hydrothermal systems, and mud volcanoes [*Van Rensbergen et al*., 2003]. The identification of surface features that could be a manifestation of subsurface sediment mobilization can therefore be an important step in understanding the geologic and atmospheric evolution of Mars.

Komatsu et al. [2016] showed that aggradational landforms inside Chryse Planitia are possibly indicative of extrusive processes associated with sedimentary volcanism. These edifices are less than a few kilometers in basal diameter and up to a few hundred meters high. *Komatsu and his co-worker*s [2016] grouped the landforms in three distinct types, i.e. cone-like features with a summit crater (Type 1), shield- or pie-like features with one or multiple summit craters (Type 2), and circular features with steep sides and a broadly flat summit area (Type 3). The study of *Komatsu et al*. [2016] focused on a small portion in the southern part of this large impact basin, roughly 70×70 kilometers in size, as this area was well covered by high-resolution images and spectral data sets enabling to study twelve edifices at small scale (for details see Tab. 1 in *Komatsu et al*. [2016]). Komatsu and colleagues suggested that such features might be spread across a wide area ranging from 16°N to 23°N and from 320°E to 326°E, however, without further investigation. Based on morphologic, morphometric, and spectral characteristics, the authors concluded that these features are a manifestation of subsurface sediment mobilization on Mars rather than igneous volcanism. Interestingly these morphology types are also very similar to those observed at mud volcanoes on Earth (see classification in *Mazzini and Etiope* [2017]). As the primary goal of *Komatsu et al*. [2016] was to reveal the formation mechanism, the full spatial extent as well as the frequency of individual types was not addressed. We searched for such edifices inside Chryse Planitia and determined their full spatial extent and the frequencies of individual types.

This enables us providing additional evidence to test the hypothesis of subsurface sediment mobilization as a possible formation mechanism.

2. Data and methods

This study is based on image data which have been obtained by the Context Camera (CTX; [*Malin et al*., 2007]) and the High Resolution Imaging Science Experiment (HiRISE; [*McEwen et al*., 2007]), both on board the Mars Reconnaissance Orbiter spacecraft, and from the High Resolution Stereo Camera (HRSC; [*Jaumann et al*., 2007]) on board Mars Express, with typical scales of 5–6 m/ pixel, ∼30 cm/pixel and 10–20 m/pixel, respectively. CTX and HRSC image data were processed with the USGS Astrogeology image processing software, Integrated System for Imagers and Spectrometers (ISIS3), and with Video Imaging Communication and Retrieval (VICAR) software provided by JPL. The images were projected in ESRI ArcGIS 10 software in a sinusoidal projection with the central meridian set at 315°E to minimize geometric distortion of studied objects. Topographic information was derived from HRSC stereo images [*Gwinner et al*., 2016] and HiRISE stereo images and derived gridded digital elevation models (DEM). While the HRSC DEM has been used to study the area of interest at regional scale, the eight HiRISE DEMs have been used to study the morphometry of 15 individual edifices of different types within the area of interest. The high-resolution DEMs were computed from HiRISE stereo pairs using the automated methods described, e.g., in *Moratto et al*. [2010].

We tested the spatial distribution of the mapped objects by using the Average Nearest Neighbor, part of the Spatial Statistics tool in ArcGIS 10. This tool enables determination of clustering or ordering by measuring the distance from every point (i.e., surface feature) to its nearest neighbor. The method is based on testing the randomness in spatial distribution by calculating the ratio between the observed mean distance and the expected mean distance for a random point distribution. If the ratio is <1, the points are clustered; the closer to zero, the more clustered [*Clark and Evans*, 1954]. The spatial distribution pattern of Type 2 objects (see section 4 for the definition of the mapped classes or types of landforms) was additionally analyzed in the R environment [*R Development Core Team*, 2011] using the Spatstat library [*Baddeley and Turner*, 2005]. At first, the distance to the nearest neighbor of each object was calculated as Euclidean point-to-point distance. The distance was then evaluated in a relationship to the object's effective radius, defined as the radius of a circle with an area equal to that of the object. The correlation of these two variables was later used to infer the spatial randomness vs. non-randomness of object distribution on shortest length scales. We also calculated the circularity of the mapped objects in an attempt to characterize their shape. Circularity was defined as the width-to-length ratios of the edifices. The widths and lengths represent the sizes of rectangular envelopes enclosing those edifices in plan view as minimum bounding geometries. Such envelopes were calculated in the ArcMap environment using the 'Minimum Bounding Geometry' tool from polygons which have been manually drawn around studied objects based on the morphological appearances of their boundaries. This method is relatively insensitive to the vertex spacing used in GIS. The resulting circularities range from 0 to 1, with 1 representing a perfect circle.

We used crater counting to reveal the absolute model ages of unit on which the studied edifices are superposed. Crater model ages were determined from crater size–frequency distributions which were measured from mosaic of CTX images in GIS environment. Only those larger than 200 meters were considered. The mapping was performed utilizing the software tool *CraterTools* [*Kneissl et al*., 2011], which ensures a distortion-free measurement of crater diameters independently from map projection. . The crater population was then analyzed by the software *Craterstats* [*Michael and Neukum*, 2010] applying the production function of *Ivanov* [2001] and the impact-cratering chronology model of *Hartmann and Neukum* [2001]. The area of crater counting is marked by white solid line on Fig. 1. The chosen area contains several large clusters of secondaries which have been manually excluded. The ages were derived using Poisson statistics to obtain a likelihood function with intrinsic uncertainty [*Michael et al*., 2016]. In the end we chose a differential crater-size frequency plot in the attempt to reveal the possible resurfacing events. A differential crater size-frequency plot shows the number of craters in each bin divided by the bin width against the crater diameter on log-log axes. Its appearance is similar to an incremental plot (number in bin vs. diameter), but with the advantage that the position of the curve on the y-scale is independent of the choice of bin-width. Like the incremental plot, it is more sensitive to resurfacing features in the distribution than a cumulative plot [*Michael et al*., 2016].

3. Geological setting

The study area (Fig. 1) is located near the southern boundary of Chryse Planitia at the terminations of the large outflow channels of Ares, Simud, and Tiu Valles. The channels were carved during the Hesperian epoch [*Tanaka et al*., 2005]. Ancient highlands are eroded into streamlined "islands", and the former floor of the channels has been resurfaced by flood deposits (and possibly volcanics [*Leverington*, 2004]), forming a relatively flat plain at elevations between -2000 m and -3900 m that slopes very gently towards north (<0.25°). These inter-island plains were previously mapped as Late Hesperian units HCc_3 and HCc_4 and Early Amazonian unit ABVm [*Tanaka et al*., 2005]. They may have been emplaced as mud flows [*Jöns*, 1990; *Ivanov et al.,* 2017], mass flow structures [*Tanaka*, 1997], and/or debris flow deposits [*Tanaka*, 1999]. Although the landing site of the Mars Pathfinder mission is located on these plains (Fig. 1), the available Pathfinder data do not enable identifying any unambiguous lithologic evidence for sedimentary rocks [*Basilevsky et al*., 1999]. Nevertheless, mud volcanism was explicitly mentioned already by *Tanaka* [1997, 1999] as a resurfacing mechanism based on the observation of small edifices in Viking Orbiter images.

4. Results

We identified 1318 edifices located in the southern part of Chryse Planitia, mapped their surface extensions and analyzed their spatial distribution. The landforms are spread over a broad area stretching from 8°N to 31°N and from 315°E to 330°E (Fig. 1), an area that is roughly three times larger than that proposed by *Komatsu et al*. [2016]. Our results reveal that the spatial distribution of these features is anticorrelated to the highlands, i.e. none of the edifices is located on the remnant streamlined highland "islands" (Fig. 1). Nearest neighbor (NN) analysis reveals that the NN ratio for all studied edifices is 0.53 (see Tab. 1 for details about the ratio for individual types) which shows a likelihood of less than 1% that their spatial distribution could be random; hence the features are clustered.

Based on the detailed investigation of twelve edifices from this large population, *Komatsu et al*. [2016] suggested that these features can be classified into three classes, cratered cones of Type 1 (Fig. 2a), shield- or pie-like features of Type 2 (Fig. 2b), and dome-shaped features of Type 3 which often have a small knob on their summit centers (Fig. 2c). Based on the mapping of our much larger area covering more edifices we defined two additional classes: Type 4 and 5. Type 4 (Fig. 2d) is characterized by a sheet-like appearance with an irregular plan shape and lobate margins. Objects are nearly flat with almost no topographical expression and typically larger than 1 kilometer in diameter, similar to Type 2 features. The surfaces of Type 4 are distinctively different from the surrounding material, as they seem to exist of two different morphologies: light, smooth material, and dark, fractured material. Type 5 features (Fig. 2e, Fig. 3a) displays a flow-like appearance commonly associated with central channels (Fig. 3b) and levees. These flow-like features can be several kilometers long and often have a central pond-like vent (Fig. 3c) from which a single channel or multiple channels originate. The closest surroundings of these channels are formed by rough elevated units of a distinct texture that is different from that of the smooth plains on which these features are superposed. While the surface of smooth plains observed at meter-scale consists of interconnected small ridges, the surface of rough elevated units consists of many small-scaled depressions around which relatively smooth surface is present (for details, see Fig. 3b in *Komatsu et al*. [2016]). The channels show a negative relief, and in some cases, an inner channel (marked with white arrow in Fig. 3d) or a highly sinuous channel can be identified (Fig. 3e). In some cases an apparent variation in the depth of the channels can be observed over the course of the flow. Channels seem to be deeper in their proximal sections close to the pond-like depressions as documented by the length of the shadows associated with the walls. The depth decreases with distance from these depressions and eventually the channels can transition into the bright units (Fig. 2e). The channels are characterized by raised rims suggesting aggradational processes associated with the flow of a material with a yield strength and its deposition [e.g., *Hulme*, 1974].

Our observations also confirm the notion of *Komatsu et al*. [2016] that features of Type 3 are associated with small knobs situated on the summit of the mounds (Fig. 4). In the time of writing 6 of these edifices were covered by HiRISE stereo-pairs which allowed us to measure the height of their knobs from resulting HiRISE DEMs. The height of such knobs is in the range of several meters (e.g., Fig. 4c),ranging from 4 m to 26 m with mean around 14 m.

Based on our mapping of 1318 edifices we found that the most common class within the study area are pie-like features of Type 2 with 679 individual members (51.5% of all observed edifices). The second most numerous class is represented by the features of Type 4 with 309 members (23.4%), followed by Type 3 (259; 19.7%), Type 1 (36; 2.7%), and Type 5 (35; 2.7%), respectively. In some cases the edifices show transitional morphologies between the defined classes. The spatial distribution based on the position of all mapped edifices shows that edifices of different types occur preferentially at specific latitudes (Fig. 1 and Fig. 5a). However, this correlation with latitude is weak and features of various types can often be observed within the same area (Fig. 3b). The only exception are edifices of Type 4 which have a tendency to occur between 11°N and 17°N. Additionally we found that features of Type 2 show a strong tendency for non-overlapping each other as shown on Fig. 5b where the nearest neighbor distance is plotted versus the feature size for all mapped Type 2 objects. Almost all data points on this image are located above the 1:1 line, which means that the nearest neighbor distance is always more than the feature size. Moreover, the most frequent nearest neighbor distances are significantly higher than the object sizes themselves. This may suggest a tendency for anti-clustering of Type 2 objects on the shortest length scales. The investigation of the circularity of Types 1-4 showed that Type 1, 2 and 3 are relatively circular (see Tab. 1 for details) with most values around 0.8 or higher (1 representing a perfect circle), suggesting that edifices of these classes are relatively axi-symmetric. Type 4 is the least circular, with most values centered on 0.7.

The age of the kilometer-sized constructional edifices is difficult to determine as they do not represent sufficiently large areas for the determination of crater size–frequency distributions (CSFD) [*Warner et al.*, 2015]. To overcome this problem, we determined the crater model ages of one unit with a known relative stratigraphic relation to the edifices, which are superposed on this unit and must therefore be younger. We obtained crater model ages for that unit of μ$880^{+0.2}_{-0.2}$ Ma, μ$1.7^{+0.2}_{-0.2}$ Ga, μ$3.2^{+0.2}_{-0.5}$ Ga, and μ$3.2^{+0.3}_{-0.8}$ Ga, respectively (Fig. 6). Note that the diameter range over the last two model ages was split because of the apparent change of isochron. The Poisson analysis however shows that, in this instance, both ranges correspond to μ3.2 Ga. This is a consequence of the downward influence of the empty binning intervals in the upper range, an effect which has been neglected in previous analyses.

These suggest that the unit experienced at least two resurfacing events affecting the populations of impact craters in different periods by repeatedly modifying the surface and hence leaving their impact on the CSFD. The studied features should be younger than those resurfacing events. It was also possible to determine the lower limit of their formation age as the investigated area is covered by clusters of secondary craters. Those clusters are ubiquitous both on highlands and lowlands and in some cases they are also overlapping edifices of our interest, hence constraining their minimum age. Mapping of the distribution of those clusters revealed that they are grouped into well-developed chains of secondary crater clusters which can be tracked to the ~55 kilometer wide and less than 5 million year old Mojave crater centered at 7.5°N and 327°E [*Werner et al*., 2014], which is known to be associated with secondary crater chains up to 1000 kilometers long that are widely spread within the area of our interest [*Werner et al*., 2014].

We also searched for the distribution of rampart craters within the study area. We observed that rampart-like ejecta within the study area are associated with impact craters with diameters of more than ~6 kilometers. They can be found both on the level plains and the remnant highlands.

5. Discussion

5.1. Morphologies

Based on our investigation of southern Chryse Planitia we confirm the morphological diversity already proposed by *Komatsu et al*. [2016], who grouped the landforms into three distinct types (Type 1-3). We additionally identified two additional classes: Type 4, represented by sheet-like features with an irregular plan shape and lobate margins, and Type 5, represented by large flow features.

The pie-like features of Type 2 that represent more than half of all observed features are characterized by circular, topographically low units (the height is limited to a few dozen meters) which are between few hundred meters up to few kilometers wide. The common presence of a central crater at these units that are associated with lobate features, interpreted by *Komatsu et al*. [2016] as flows emanating from these craters, together with the well-developed lobate margins of these units and the ability of the material forming these low units to infill local depressions (e.g., fractures) suggest that some sort of low-viscosity material has been expelled from a central crater and then laterally spread over the flat plains. The features of Type 3 that comprise around one fifth of all observed features are represented by cones with relatively flat summit areas on which small knobs are superposed. Their circularity, the gradual transition into the surrounding plains, and the absence of fracture patterns such as radial faults (which would possibly hint at an intrusive emplacement; see also below) suggest that also these features have been formed by the ascent of material from the subsurface. However, the small lateral extensions of these features together with the low heights of several dozens of meters suggest that the extruded liquid had to be of relatively higher-viscosity than in the case of features of Type 2. On the other hand, the few crater-like features of Type 1 on the other hand do not often show direct evidences of flow-like patterns. Instead they show well-developed central craters where layering of the inner rim walls can be observed [*Komatsu et al*., 2016]. Their relatively pristine shapes suggest that they are not erosional remnants, but instead have been formed by accumulation of material in the vicinity of the central crater.

We observed 309 edifices of Type 4 to be distributed within the mouth regions of the outflow channels at a specific range of latitudes and topographic elevations in the southern part of our study area (Fig. 1 and Fig. 4a). Their surface textures are distinctively different from that of the surrounding material, which enables their detection; however, they do not show any morphological characteristics that can be directly associated with the subsurface sediment mobilization. However, a genetic link between features of Type 4 and features of other types can be inferred from their spatial association (Figs. 1 and 4a), as Type 4 features commonly share the same geographic area with features of other types, suggesting that they may have been formed by a similar mechanism. The lack of clear morphological characteristics which may reveal how these features have been formed prevents us from speculating about their origin. However, their localized distribution at specific latitudes may suggest that, for example, a certain thickness range of sedimentary strata may play a critical role in their formation.

On the other hand, Type 5 features are indicative of flow processes. One of these landforms was already observed by *Komatsu et al*. [2016]. However, as it was a unique feature within their mapping area it was not defined as a separate morphological class. We observed a total of 34 examples of Type 5 features which enables us describing their general morphology. They are formed by three distinct parts: (i) a central pond-like depression from which a channel or channels are spreading into the surroundings (Fig. 2e), (ii) a part of the channel which may or may not have incised into the substrate (though there is no unambiguous evidence for erosion) (Fig. 3d), and (iii) a part of the channel in which deposition dominates and the channel gradually disappears into the surrounding plain without leaving behind any significant topographical signature at the end of the flow (Fig. 3e). Such variations in morphology are consistent with the extrusion of a low-viscosity material from the subsurface in the area of the pond-like depression, followed by subsequent transport of the material as a liquid via a network of channels and by a gradual loss of the ability of the flow to carry the material (e.g., an increase of viscosity) and hence deposition of sediments across the flat plains. Additionally, the presence of an inner channel (marked with a white arrow on Fig 3d) suggests that the amount of flowing liquid decreased with time. Similarly as features of Type 4, Type 5 features are also spatially associated with features of other types, suggesting a genetic link between them (Fig. 3b).

Based on our work we therefore found that most of the observed morphologies are consistent with the effusive emplecement of material with low viscosity capable of lateral movement over kilometer-scale distances. In many cases, transitional morphologies or a direct spatial association of different types (as for example shown on Fig. 3a) may indicate that features of all classes share a similar causal mechanism of their formation. Our observations are therefore consistent with the idea that the features are the result of subsurface sediment mobilization as proposed by *Komatsu et al*. [2016].

5.2. Spatial distribution

The analysis of their spatial distribution shows that the investigated edifices are strictly anticorrelated with the highlands (Fig. 1) as they occur exclusively on the level plains. As these level plains are composed by sedimentary deposits interpreted to have formed by rapidly emplaced fluvial sediments and/or debris flows associated with outflow channels [*Tanaka et al*., 2005], this observation favors subsurface sediment mobilization over igneous volcanism as a possible mechanism for their formation. Although it is known that the presence of igneous edifices can be associated with sedimentary depocentres both on Earth and Mars [e.g., *Kereszturi and Németh*, 2013; *Brož et al*., 2015; 2017], the complete absence of the investigated edifices on the highlands suggests that the existence of sediments is a necessary condition for the formation of the edifices in southern Chryse Planitia. If the huge area characterized by the edifices were an igneous volcanic province, it should be expected that at least some volcanic features should have formed on the remnant highlands. The observed elevation difference between the sedimentary plains and the tops of the highland remnants is only a few dozens of meters up to 500 meters (Fig. 7). It would be an unlikely coincidence if buoyantly ascending magma would have been able to reach the surface in the plains area, but not at the slightly higher erosional remnants of the highlands because the level of neutral buoyancy (i.e. the crustal level below which the country rocks are denser than the magma; e.g., *Walker* [1989]; *Lister and Kerr* [1991]) would be located just in that narrow elevation range. The fact that buoyance is a volume force and, therefore, dikes may overshoot above the level of neutral buoyancy [*Taisne and Jaupart*, 2009] and reach even higher elevations would further decrease the likelihood that buoyancy would limit igneous volcanism to the plains regions.

We also considered a second reason that may lead to a preferential localization of volcanism in lowlands. It has been shown that magma ascending in a dike whose strike runs across topographic relief tends to be diverted away from the highlands [*Gaffney and Damjanac*, 2006]. This is due to two effects. First, the higher laterally confining stress beneath the highlands tends to limit the dike aperture to a higher degree than beneath the lowlands. Second, when ascending magma reaches the surfaces in the lowlands, the pressure release in the dike would prevent further rise of the portion of the dike beneath the highlands (see inset in Fig. 7a for a graphical illustration of this effect). The modelling of *Gaffney and Damjanac* [2006] showed that the first effect is generally much smaller than the second one, and even the latter does not preclude magma to reach elevations above the plains level. Moreover, this applies only to dikes which cut the transition between lowlands and highlands. In theory, an absence of feeder dikes on the highland "islands" might also occur if dikes paths were systematically deflected from a vertical orientation beneath the highlands, thus forming sills. However, this would be expected if the ascending dike meets a more rigid medium [e.g., *Maccaferri et al*., 2010; *Gudmundsson*, 2011], but there is little reason to assume that the regolith that comprises the uppermost crust in the highlands is mechanically more rigid than the material below. Instead, there is geophysical evidence from topography and gravity data that the density of the Martian crust increases with depth [*Goossens et al*., 2017].

We therefore conclude that igneous volcanism in the study area would likely have left traces both on the highlands and the lowlands (Fig. 7a). The most plausible explanation for the observed spatial dichotomy in the distribution of the landforms is therefore a direct link to the sedimentary plains, which seem to be the source for the extruded material (Fig. 7b), rather than any deep-seated magma reservoirs.

An additional problem for an igneous interpretation of the mapped landforms is posed by the presence of subsurface volatiles. The distribution of rampart craters on the highlands and on the smooth plains (marked by blue polygons in Figure 1) is evidence for subsurface water and/or ice across the investigated area [e.g., *Jones et al*., 2016]. Moreover, specific morphological features such as a lobate-shaped ejecta blanket, numerous pits on the crater floor, and the fluvial landforms in the crater interior associated with the young (< 5 Ma) Mojave crater suggest that volatiles may persist in the subsurface even in the very recent past [*Werner et al*., 2014]. Any ascending magma should have had therefore ample oportunities to interact with the volatiles, giving rise to explosive hydrovolcanic eruptions. This would lead to the formation of specific surface landforms, such as lineated depressions, rootless cones, or clusters of volcanic craters which have been previously observed elsewhere on Mars [e.g., *Wilson and Head*, 2004; *Lanagan et al*., 2001; *Brož and Hauber*, 2013]. Despite specifically searching for such evidence of phreatomagmatic processes, we identified only 36 out of 1318 edifices (classified as the Type 1) that are cones with large and deep central craters and could be explained by explosive activity. These features therefore represent only a minor fraction of the total population within the study area. On the contrary, the most frequent morphologic class is represented by the pie-like edifices of Type 2 (N=679), which often display small central craters with lobate features interpreted to be flows emanating from these craters. We suggest that most material was therefore extruded from the subsurface to the surface by effusion rather than by explosions (see details below). The fact that pie-like features of Type 2 can be found in areas where the presence of rampart craters is documented suggests that effusive activity occurred in volatile-rich areas where ideal conditions for phreatomagmatic explosive eruptions would been met. The scarcity of possible phreatomagmatic landforms is therefore difficult to reconcile with an igneous scenario.

This is also the case for the spatial distribution of the observed edifices at local scale. Despite the fact that the features show a tendency to cluster (Fig. 1), they are rarely overlapping each other within such clusters (Fig. 5b), and typically do not form edifices with multiple vents (with the exception of Type 2 features, however, even in this case the vents are overlapping each other only in the case of few individual edifices). Both edifice coalescence and the existence of multiple vents are frequent phenomena in monogenetic volcanic fields on Earth containing hundreds of volcanic edifices [*Kereszturi and Németh*, 2013]. Similar characteristics have also been observed for kilometer-sized pitted cones on Mars which have been hypothesized to be igneous volcanoes [*Brož and Hauber*, 2012; 2013; *Brož et al*., 2017]. Instead the spatial distribution of the studied edifices and the lack of coalescence suggest that there is a minimum threshold area (and likely volume) which is required for an individual edifice to form (Fig. 5b).

5.3. Stability of the mud in the Martian environment and the effect on the shapes of observed features

Based on a comparison with terrestrial mud volcanoes in Azerbaijan and Pakistan, *Komatsu et al*. [2016] proposed that the observed surface features may represent the results of the extrusion (Type 1, 2 and one large flow edifice) and intrusion (Type 3) of mud onto and into the upper crust of Mars, respectively. Following the work of *Lance et al*. [1998], *Komatsu et al*. [2016] proposed that the observed wide morphological diversity of the features may be explained in terms of material properties and the shape of the feeder dike conduit. Material properties such as viscosity affect the rheological behavior of such mixture and the way how it flows, and the shape of the feeder conduit can change the relative size of the shear zone, affecting the temperature [*Mastin*, 2002] and the degree of fluidization of thixotropic mud [*Lance et al*., 1998]. Furthermore, *Komatsu et al*. [2016] suggested that other factors such as the proportion of solid clasts in the mud matrix, water content, or the eruption rate of the mud also control the final shape of the edifices and flows.

When assessing the relative importance of these factors, the different environmental conditions at the Martian surface (as compared to Earth) also needs to be considered. Subsurface sediment mobilization on Mars (if once present) would lead to the expulsion of a water-sediment mixture into an ambient low-pressure atmosphere, in which liquid water is not stable for prolonged periods of time [e.g., *Hecht*, 2002; *Bargery et al*., 2010]. The behavior of such a mixture on Mars probably would therefore differ from that on Earth, and substantial morphologic differences of mud mounds among Mars and Earth may be expected.

Recent experiments performed in a vacuum chamber indeed showed that mixtures of liquid water and sediment behave differently than expected if exposed to a Mars-analogue low pressure environment [e.g., *Conway et al*., 2011; *Massé et al*., 2016; *Raack et al*., 2017]. Such mixtures also have a different capability in comparison to terrestrial conditions to modify the surface by erosion and deposition, or to activate further processes which are not operating at normal circumstances on Earth. For example, *Conway et al*. [2011] observed that water at low temperature and low pressure has a greater erosion capacity and flows faster over a sand bed causing an increase in the runout distance of such flows. Based on these findings they predict that fluvial flow features on Mars could be formed by volumes of liquid an order of magnitude less than for similar flow lengths on Earth. *Massé and her co-workers* [2016] further discovered that the transport mechanism can be affected, too. The instability of water causes its boiling as it percolates into the sediment, inducing grain saltation, the construction of small aggradational ridges and subsequent slope destabilization; hence additional sediment transport by dry mass wasting would occur. This means that on Mars, a hybrid flow mechanism involving both wet and dry processes may be operating and more material could be transported than would be possible on Earth with the same amount of water. Similarly, *Raack et al*. [2017] observed that the saturation of sediment on inclined slopes can even lead to a new type of material transport, i.e. levitation of water-saturated sediment bodies on a cushion of vapor released by boiling. Due to this process the volume of material which can be transported increases even though less water may be available. These findings all point to the likelihood that the movement of mud flows in the Martian environment would behave differently than perhaps expected.

5.4. Formation of the observed features

We therefore consider a scenario that is based on that proposed by *Komatsu et al*. [2016], but modified with respect to the control of the Martian environment on the behavior of the mud and hence on the final shape of the features. In our conceptual model the differences in observed shapes (with the exception of Type 4 where the lack of distinct morphology does not enable us inferring their formation in detail) can be then attributed to variations in the water content within the mud – affecting its viscosity and hence its ability to flow – and to variations in the effusion rates of such mixture or a combination thereof (Fig. 8).

In our scenario, the large flow features of Type 5 are the results of the ascent, eruption, and the subsequent movement over the surface of a relatively large quantity of a low-viscosity liquid in a short period of time. Hence these features would represent an end member in terms of the viscosities, extruded volumes, and effusion rates. We propose that the low viscosity could be caused by a large amount of water within the mixture enabling it moving relatively easily over large distances. We suggest that mud was extruded on the surface in the pond-like depressions from where it would propagate to the surroundings following the topographical gradient. The large quantity of the extruded highly mobile mixture would be able to carry the material away and hence would form the kilometer-long network of channels. As the amount of the extruded mud would not be steady over time, but would be declining as the subsurface reservoir would be getting depleted, this would cause the formation of the inner channels observed within those flow-like features (marked with white arrow in Fig. 3d).

As the water mixture would be extruded into the Martian low pressure-environment in which liquid water is unstable for prolonged periods of time, we expect that the water would have started to evaporate to the surrounding atmosphere [*Bargery and Wilson*, 2010]. An additional loss of water would be caused by the infiltration of water into the sediment over which the material propagated [sieve deposition; *Hooke*, 1967; *Milana*, 2010]. It has to be noted, however, that the lower gravity on Mars and the refreezing of infiltrated water in the top layers of a cold substrate [*Pfeffer and Humphrey*, 1998; *McCauley et al*., 2002; *Conway et al*., 2011] will limit the efficiency of water loss by infiltration. Moreover, mud flows are characterized by a low diffusivity and can therefore retain their water for a long time. Nevertheless, any water loss by whatever mechanism would cause a decrease in the sediment transport capacity of the mud flow with time and distance from the vent. At a certain stage, transport of the material would be replaced by deposition as the dominant process. We therefore propose that two distinct morphologies would therefore be formed over the length of the flow-like features: one dominated by transport and the other by deposition. Landforms associated with transport would be channels with little material deposited off the channel whereas areas dominated by deposition would be characterized by bright units spreading out from central channels. We assume that infiltration of the water into the surrounding sedimentary rocks, although perhaps not an efficient mechanism on Mars, together with subsequent evaporation and sublimation of water and ice, respectively, may be then responsible for the volume loss and the formation of, e.g., sublimation pits, creating the rough elevated units surrounding the close vicinity of the pond-like vents and channels.

A decreasing water content in the mud would increase its viscosity [*Lee and Widjaja*, 2013], and the movement across the surface would be more difficult. We therefore propose that pie-like features of Type 2 are the results of relatively lower effusion rates as compared to Type 5 features, accompanied with a viscosity increase caused by a lower water content of the extruding mud. As the consequence the mixture would be spread over smaller areas than in the case of Type 5. However, as the final pie-like features are relatively flat – their maximum heights are only few dozens of meters – the mud would still have to have a relatively low viscosity. The presence of small central craters leads us to conclude that the material had to come to the surface from below and then laterally spread around the vent. Lateral spreading of extruded material is also supported by the relatively high circularity (i.e. axisymmetry) of these features; a common plan-view shape for bodies formed by the flow of some type of liquid on relatively flat plains [*Turcotte and Schubert*, 2002, p. 387]. The instability of water in the mud would cause its boiling and hence would allow formation of bubbles of water vapor which would leave the mixture explosively in the form of small bursts. These bursts would be capable of forming a large quantity of submetre-scale craters and hence would give rise to observed hummocky texture of the pie-like units as already proposed by *Komatsu et al*. [2016]. We hypothesize that this phenomenon is associated with the viscosity of mud which would affect the ability of bubble coalescing and exiting the mixture. If the viscosity is too low, even small bubbles would easily escape the mixture and hence they would not have time to coalesce and form large bubbles creating submetre-scale craters. If the viscosity is too high, the bubbles may not be able to merge into large bubbles as the mixture would not be easily permeable for them and this would again preclude the formation of such hummocky surface texture.

Additional decrease of the water content within the mud, again associated with an increasing viscosity of such mixture and a continuing decrease in effusion rates can would then explain the formation of Type 1 features. The decrease in effusion rates would cause the mud spending more time in the feeder conduit so large gas bubbles may form and coalesce together [e.g., *Vanderkluysen et al*., 2014]. These bubbles would then trigger explosive bursts of the mud in a similar fashion as volcanic gasses trigger Strombolian or Vulcanian eruptions in the case of silicic magma [*Gonnermann and Manga*, 2007; *Tran et al*., 2015]. The mud fragments would be then transported by ballistic pathways [*Vona et al*., 2015] to the vicinity of the conduit where those fragments would accumulate into conical edifices with a large central crater. Such a process is also known to operate in the case of gas-rich mud volcanoes on Earth [e.g., *Mazzini and Etiope*, 2017]. However, because the atmospheric pressure on Mars is lower than on Earth, such eruptions would vary in several aspects from those known from Earth. Firstly, explosive bursts would be more energetic than those on Earth, as the gas would expand more rapidly in the low pressure environment, similar to volcanic gasses [e.g., *Wilson and Head*, 1994]. Ballistically ejected material would therefore be able to travel faster and further than on Earth [*Brož et al*., 2015]. The final width of the mud cone and the crater could be therefore larger than what is typical on Earth. Moreover, the physical instability of liquid water would cause the mud desiccating once ejected into the Martian atmosphere. This might prohibit the mixture coalescing into a mud flow after the deposition, and the final sedimentary volcanic landforms may therefore be emplaced ballistically only, and not associated with lateral movement by flows as common for sedimentary volcanism on Earth [e.g., *Mazzini and Etiope*, 2017]. This would explain the absence of flow-like features associated with Type 1 edifices.

An even lower water content in the mud would imply an additional increase in viscosity, hence highly immobile mud unable of any significant lateral movement may be generated. We suggest that if such material were extruded on the surface of Mars, it would accumulate in close vicinity of the feeder conduit. A domical landform with steep flanks would be formed in similar way as highly viscous lava is giving rise to lava domes [*Fink and Griffiths*, 1998]. We therefore propose that the domical features of Type 3 result from the extrusion of such highly viscous mud on the surface instead of mud intrusions as previously proposed by *Komatsu et al*. [2016]. In the scenario of Komatsu et al. these domes should be formed by mud emplacement underneath an old sedimentary volcano or other surficial edifices without major mud eruption. However, no fracture patterns such as radial faults as expected above domical intrusions or mud injections [e.g., *Withjack and Scheiner*, 1982; *Jackson and Pollard*, 1990; *Yin and Groshong*, 2007; *Aranda-Gómez et al*., 2016] are observed. The domes also have small central knobs on their summit plateaus (Fig. 2c), which *Komatsu et al*. [2016] interpreted as vent structures made of accumulated sediment, similar to terrestrial gryphons. Whereas we cannot rule out this possibility, we propose an alternative explanation taking into account the environmental properties on Mars, which would support an effusive scenario for these domes. In their investigation of lunar irregular mare patches, *Wilson and Head* [2017] found that in environments with negligible atmospheric pressure very late-stage volatile release could form very vesicular lava "foams" during the terminal stages of lunar shield volcanic eruptions. This process may form very peculiar morphological features when such foam is extruded onto the solidified crust of a lava lake, forming mounds with very high porosity. Because highly viscous mud would behave in many aspects similarly as silicic lava, we therefore hypothesize that the volume change at the terminal stage of subsurface sediment mobilization and mud ascent could lead to the formation of small knobs (Fig. 2c) in a similar manner as lava foams accumulated on the surface of the Moon. The volume of mud trapped in the conduit would increase as the gas bubbles within the highly viscous mud would expand, causing subsequent extrusion of a small amount of the material on the surface and hence the formation of these small knobs. The position of this feature would then mark the position of the feeder conduit.

Our model also explains the formation of the different types of mapped features, also accounting for transitional morphologies as the process is likely to be much more complex in reality. The amount of water within the mud (hence the viscosity of the extruded material) would change over the course of the eruption so the final morphologies would reflect such change. However, we acknowledge that the proposed scenario has its limitations. The lack of morphological details of Type 4 does not allow us to explain the formation of these edifices. It is also uncertain if mud can actually propagate over the surface of Mars; no experimental work has been done on this topic yet, although *Wilson and Mouginis-Mark* [2014] have explored the flow of mud on Mars theoretically. Further laboratory work in simulation chambers in which mud would be exposed to the low Martian atmospheric pressure conditions would be required to better assess the mechanisms of mud eruption and transport on Mars.

5.5. Geologic Implications

In analogy to terrestrial outflow events (e.g., from jökulhlaups or the catastrophic drainage of ice-dammed lakes), *Rice and Edgett* [1997] proposed a sandar facies model for southern Chryse Planitia to predict some characteristics of the Pathfinder landing site. Their model distinguishes three facies types (proximal, midfan, and distal facies) in a lateral sequence from South to North. Most of the features mapped in this study are located in the zone of the midfan facies. We tested the hypothesis that the different feature types mapped in this study have been sourced from sedimentary facies emplaced in different depositional environments. Such a correlation of sedimentary volcanic feature type with basin-related location (i.e. proximal to distal) has been suggested for neighboring southern Acidalia Planitia [*Salvatore and Christensen*, 2015; *Orgel et al*., 2018]. However, with the exception of Type 4 features, which are least constrained with respect to the water content of their source material and the related effusion rates, there is no clear correlation of feature type with latitude or distance to outflow channel termini (Fig. 1 and 5a). It is therefore not possible to explain the variations of water content and effusion rates of the features as a simple function of proximal vs. distal sedimentary facies if the features were formed simultaneously from the same sedimentary source. However, it is unknown from which depth the expulsed sediment comes from. The sedimentary environment at a given location evolved during the duration of outflow event(s) and may have led to a complex stratigraphy. For example, the same geographic position may have first represented a distal and later a proximal facies, which would eventually be located in lower and higher stratigraphic positions, respectively. Such a sedimentary architecture may have favored the release of sedimentary volcanic material with different water content and effusion rates from different depths, perhaps even at the same time (see inset C in Fig. 7b). A complex stratigraphy of Chryse Planitia has indeed been independently suggested on the basin of layered impact crater ejecta characteristics [*Jones et al*., 2016]. A stack of sedimentary layers containing substantial portions of mud [*Jöns*, 1985] and some volcanic material [*Scott and Tanaka*, 1986], possibly hosting aquifers [*Rodríguez et al*., 2007] and ice layers or lenses [*Carr and Head*, 2019] would be a plausible source for liquefaction, subsurface sediment mobilization and sedimentary volcanism.

The presence of secondary craters associated with the Mojave impact suggest that the observed features are more than 5 million years old [*Werner et al*., 2014], possibly dating back much further to the period following outflow channel formation. It is therefore unlikely that outgassing of the source sediments is still active. Although processes associated with subsurface sediment mobilization are often proposed as the possible source of atmospheric methane [e.g., *Oehler and Etiope*, 2017], our findings do not support a direct link of the formation of the studied features to the atmospheric methane that has been recently reported [*Webster et al*., 2018].

6. Conclusions

We investigated a large field of kilometer-sized cone- and pie-like landforms in southern Chryse Planitia on Mars, which have been previously interpreted as mud volcanoes [*Tanaka*, 1999; *Komatsu et al*., 2016]. The features show a larger morphological variety than previously recognized, and five different types can be distinguished (two more than identified by *Komatsu et al*. [2016]). The morphologies indicate a formation mechanism related to the extrusion of a water-rich sediment expelled from the subsurface. The entire population consists of more than 1300 features which are spread over an area of circa 700,000 km^2. Mapping of their spatial distribution shows that the landforms are exclusively located in the sedimentary plains between erosional remnants (“streamlined islands”) of the ancient highlands suggesting a formation mechanism that is directly linked to sediments. We favor a formation by subsurface sediment mobilization and sedimentary volcanism, as igneous volcanic flows and edifices would likely be located on both the sedimentary plains and the interspersed remnant highlands.

We hypothesize that the morphological variety among the studied features can be explained by the variability of the water content of the ascending mud and by the variability in the effusion rates. Large flow-like features would thus be a result of the extrusion of large amounts of water-rich mud of low viscosity capable to travel over large distances. Lower water content would cause a viscosity increase and hence the formation of the most numerous features within this region, pie-like features. On the other hand the presence of cone- and dome-like features suggests that highly viscous mud was also extruded within the study area. Except of Type 4 there is no clear correlation of feature type with distance to outflow channel termini. Although the different landforms may be sourced from different depths, representing different sedimentary facies during outflow channel evolution, the available data do not enable constraining the possibly complex subsurface stratigraphy.

Therefore this area represents an interesting candidate landing site as the proposed sedimentary volcanoes would enable to investigating subsurface sediment strata [*Parnell et al*., 2009] and hence revealing details about the evolution of Chryse Planitia and other Martian basins infilled by sediments.

Fluidization of sediments, recently also inferred from ground observations through rovers [*Rubin et al*., 2017], may have been a geologically important process on Mars. It is important to note, however, that Earth-based models may not be reliable predictors of the morphology of landforms resulting from Martian sedimentary volcanism. Several morphological characteristics such as a hummocky texture associated with Type 2, interpreted to be the result of water evaporation/ice sublimation, and the presence of small central knobs on top of Type 3 features, interpreted to be a result of late-stage expansion of a mud-gas bubble mixture in the ambient low pressure atmosphere, suggest that specific Martian environmental conditions significantly affected the behavior of the extruded mud. Environmental factors should be therefore considered in further studies of subsurface sediment mobilization and extrusion on Mars, including experimental investigations in Mars simulation chambers.

7. References

Allen, C. C., D. Oehler, G. Etiope, P. Van Rensbergen, C. Baciu, A. Feyzullayev, G. Martinelli, K. Tanaka, and D. Van Rooij (2013), Fluid expulsion in terrestrial sedimentary basins: a process providing potential analogs for giant polygons and mounds in the martian lowlands, *Icarus* 224, 424–432. https://doi.org/10.1016/j.icarus.2012.09.018.

Aranda-Gómez, J. J., M. Cerca, L. Rocha-Treviño, J. J. Carrera-Hernández, G. Levresse, J. Pacheco, V. Yutsis, J. A. Arzate-Flores, E. Chacón, and H. Beraldi-Campesi (2016), Structural evidence of enhanced active subsidence at the bottom of a maar: Rincón de Parangueo, México, In: Németh, K., Carrasco-Núñez, G., Aranda-Gómez, J. J. & Smith, I. E. M. (eds) Monogenetic Volcanism. Geological Society, London, Special Publications, 446(1), 225–254. http://dx.doi.org/10.1144/sp446.1.

Baddeley A., and R. Turner (2005), Spatstat: An R package for analyzing spatial point patterns, *Journal of Statistical Software* 12, 1–42. http:// doi.org/10.18637/jss.v012.i0.

Bargery, A. S., and L. Wilson (2010), Dynamics of the ascent and eruption of water containing dissolved CO_2 on Mars, *J. Geophys. Res.* 115, E05008. https://doi.org/10.1029/2009JE003403.

Bargery, A.S., S. J. Lane, A. Barrett, L. Wilson, and J. S. Gilbert (2010), The initial responses of hot liquid water released under low atmospheric pressures: Experimental insights, *Icarus* 210, 488–506. http://dx.doi.org/10.1016/j.icarus.2010.06.019.

Basilevsky, A. T., W. J. Markiewicz, N. Thomas, and H. U. Keller (1999), Morphologies of rocks within and near the Rock Garden at the Mars Pathfinder landing site, *J. Geophys. Res*. 104(E4), 8617–8636. http://dx.doi.org/10.1029/1998JE900039.

Brož, P., and E. Hauber (2012), A unique volcanic field in Tharsis, Mars: pyroclastic cones as evidence for explosive eruptions, *Icarus* 218, 88–99. http://dx.doi.org/10.1016/j.icarus.2011.11.030.

Brož, P., and E. Hauber (2013), Hydrovolcanic tuff rings and cones as indicators for phreatomagmatic explosive eruptions on Mars, *J. Geophys. Res. Planets* 118, 1656–1675. http://dx.doi.org/10.1002/jgre.20120.

Brož, P., O. Čadek, E. Hauber, and A. P. Rossi (2015), Scoria cones on Mars: detailed investigation of morphometry based on high-resolution digital elevation models, *J. Geophys. Res. Planets* 120, 1512–1527. http://dx.doi.org/10.1002/2015JE004873.

Brož, P., E. Hauber, J. J. Wray, and G. Michael (2017), Amazonian volcanism inside Valles Marineris on Mars, *Earth and Planetary Science Letters* 473, 122–130. http://dx.doi.org/10.1016/j.epsl.2017.06.003.

Carr, M., and J. Head (2019), Mars: Formation and fate of a frozen Hesperian ocean, *Icarus* 319, 433–443. https://doi.org/10.1016/j.icarus.2018.08.021.

Clark, P. J., and F. C. Evans (1954), Distance to nearest neighbour as a measure of spatial relationships in populations, *Ecology* 35, 445–453. http://dx.doi.org/10.2307/1931034.

Conway, S. J., M. P. Lamb, M. R. Balme, M. C. Towner, and J. B. Murray (2011), Enhanced runout and erosion by overland flow at low pressure and subfreezing conditions: experiments and application to Mars, *Icarus* 211, 443–457. https://doi.org/10.1016/j.icarus.2010.08.0266.

Fink, J. H., and R. W. Griffiths (1998), Morphology, eruption rates, and rheology of lava domes: insights from laboratory models, *J. Geophys. Res.* 103(B1), 527–545. http://dx.doi.org/10.1029/97JB02838.

Formisano, V., S. Atreya, T. Encrenaz, N. Ignatiev, and M. Giuranna (2004), Detection of methane in the atmosphere of Mars, *Science* 306, 1758–1761. http://dx.doi.org/10.1126/science.1101732.

Gaffney, E. S., and B. Damjanac (2006), Localization of volcanic activity: Topographic effects on dike propagation, eruption and conduit formation, *Geophys. Res. Lett*. 33, L14313. https://doi.org/10.1029/2006GL026852.

Geminale, A., V. Formisano, and G. Sindoni (2011), Mapping methane in martian atmosphere with PFS-MEX data, *Planet Space Sci*. 59, 137–148. https://doi.org/10.1016/j.pss.2010.07.011.

Gonnermann, H.M., and M. Manga (2007), The fluid mechanics inside a volcano, *Ann. Rev. Fluid Mech*. 39, 321–356. https://doi.org/10.1146/annurev.fluid.39.050905.110207.

Goossens, S., T. J. Sabaka, A. Genova, E. Mazarico, J. B. Nicholas, and G. A. Neumann (2017), Evidence for a low bulk crustal density for Mars from gravity and topography, *Geophys. Res. Lett.* 44, 7686–7694. https://doi.org/10.1002/2017GL074172.

Gudmundsson, A. (2011), Deflection of dykes into sills at discontinuities and magma-chamber formation, *Tectonophysics* 500, 50-64. https://doi.org/10.1016/j.tecto.2009.10.015.

Gwinner, K., R. Jaumann, E. Hauber, H. Hoffmann, C. Heipke, J. Oberst, G. Neukum, V. Ansan, J. Bostelmann, A. Dumke, S. Elgner, G. Erkeling, F. Fueten, H. Hiesinger, N. M. Hoekzema, E. Kersten, D. Loizeau, K.-D. Matz, P. C. McGuire, V. Mertens, G. Michael, A. Pasewaldt, P. Pinet, F. Preusker, D. Reiss, T. Roatsch, R. Schmidt, F. Scholten, M. Spiegel, R. Stesky, D. Tirsch, S. van Gasselt, S. Walter,M. Wählisch, and K. Willner (2016), The High Resolution Stereo Camera (HRSC) of Mars Express and its approach to science analysis and mapping for Mars and its satellites, *Planetary and Space Science* 126, 93-138. http://dx.doi.org/10.1016/j.pss.2016.02.014.

Hartmann, W. K., and G. Neukum (2001), Cratering chronology and the evolution of Mars, *Space Sci. Rev*. 96 (1/4), 165–194. http://dx.doi.org/10.1023/A:1011945222010.

Hecht, M. H. (2002), Metastability of liquid water on Mars, *Icarus* 156, 373-386. https://doi.org/10.1006/icar.2001.6794.

Hemmi, R., and H. Miyamoto (2018), High-Resolution Topographic Analyses of Mounds in Southern Acidalia Planitia, Mars: Implications for Possible Mud Volcanism in Submarine and Subaerial Environments, *Geosciences* 8(5), 152. https://doi.org/10.3390/geosciences8050152.

Hulme, G. (1974), The interpretation of lava flow morphology, *Geophys. J. R. Astr. Soc*. 39, 361–83, https://doi.org/10.1111/j.1365-246X.1974.tb05460.x.

Hooke, R. L. (1967), Processes on arid-region alluvial fans, *Journal of Geology* 75, 438–460. http://dx.doi.org/10.1086/627271.

Ivanov, M. A. (2001), Mars/Moon cratering rate ratio estimates, *Space Sci. Rev*. 96, 87–104. http://dx.doi.org/10.1023/A:1011941121102.

Ivanov, M. A., G. Erkeling, H. Hiesinger, H. Bernhardt, and D. Reiss (2017), Topography of the Deuteronilus contact on Mars: Evidence for an ancient water/mud ocean and long-wavelength topographic readjustments, *Planetary and Space Science* 144, 49–70. http://dx.doi.org/10.1016/j.pss.2017.05.012.

Jackson, M. D., and D. D. Pollard (1990), Flexure and faulting of sedimentary host rocks during growth of igneous domes, Henry Mountains, Utah, *Journal of Structural Geology* 12, 185–206. http://dx.doi.org/10.1016/0191-8141(90)90004-I.

Jaumann, R., et al. (2007), The high-resolution stereo camera (HRSC) experiment on Mars Express: instrument aspects and experiment conduct from interplanetary cruise through the nominal mission, *Planet. Space Sci*. 55, 928–952. http://dx.doi.org/10.1016/j.pss.2006.12.003.

Jöns, H.-P. (1985), Late sedimentation and late sediments in the Northern Lowlands on Mars, *Lunar and Planetary Science* XVI, 414-415 (abstract).

Jöns, H.-P. (1990), Das Relief des Mars' - Versuch einer zusammenfassenden Übersicht (Teil III), *Geologische Rundschau* 79/1 I, 131–164. http://dx.doi.org/10.1007/BF01830452.

Jones, E., G. Caprarelli, and G. R. Osinski (2016), Insights into complex layered ejecta emplacement and subsurface stratigraphy in Chryse Planitia, Mars, through an analysis of THEMIS brightness temperature data, *J. Geophys. Res. Planets* 121, 986–1015. http://dx.doi.org/10.1002/2015JE004879.

Kereszturi, G., and K. Németh (2013), Monogenetic basaltic volcanoes: genetic classification, growth, geomorphology and degradation. In: Nemeth, K. (Ed.), Updates in Volcanology – New Advances in Understanding Volcanic Systems, 3–89, InTechOpen. https://doi.org/10.5772/51387.

Kneissl, T., S. van Gasselt, and G. Neukum (2011), Map-projection-independent crater size-frequency determination in GIS environments – new software tool for ArcGIS, *Planet. Space Sci*. 59, 1243–1254. http://dx.doi.org/10.1016/j.pss.2010.03.015.

Komatsu, G., C. H. Okubo, J. J. Wray, L. Ojha, M. Cardinale, A. Murana, R. Orosei, M. A. Chan, J. Ormö, and R. Gallagher (2016), Small edifice features in Chryse Planitia, Mars: assessment of a mud volcano hypothesis, *Icarus* 268, 56–75. http://dx.doi.org/10.1016/j.icarus.2015.12.032.

Kopf, A. J. (2002), Significance of mud volcanism, *Rev. Geophys.* 40(2), 1005. http://dx.doi.org/10.1029/2000RG000093.

Krasnopolsky, V. A. J. P. Maillard, and T. C. Owen (2004), Detection of methane in the martian atmosphere: Evidence for life?, *Icarus* 172, 537–547. https://doi.org/10.1016/j.icarus.2004.07.004.

Lanagan P. D., A. S. McEwen, L. P. Keszthelyi, and T. Thordarson (2001), Rootless cones on Mars indicating the presence of shallow equatorial ground ice in recent times, *Geophys. Res. Lett*. 28(12), 2365-2367. https://doi.org/10.1029/2001GL012932.

Lance, S., P. Henry, X. Le Pichon, S. Lallemant, H. Chamley, F. Rostek, J.-C. Faugeres, E. Gonthier, and K. Olu (1998), Submersible study of mud volcanoes seaward of the Barbados accretionary wedge: Sedimentology, structure and rheology, *Mar. Geol.* 145, 255–292. https://doi.org/10.1016/S0025-3227(97)00117-5.

Lee, S. H.-H., and B. Widjaja (2013), Phase concept for mudflow based on the influence of viscosity, *Soils and Foundations* 53, 77–90. http://dx.doi.org/10.1016/j.sandf.2012.12.005.

Leverington, D. W. (2004), Volcanic rilles, streamlined islands, and the origin of outflow channels on Mars, *J. Geophys. Res.*, 109, E10011, doi:10.1029/2004JE002311.

Lister, J. R., and R. C. Kerr (1991), Fluid-mechanical models of crack propagation and their application to magma transport in dykes, *J. Geophys. Res.* 96(B6), 10049–10077. https://doi.org/10.1029/91JB00600.

Maccaferri, F., M. Bonafede, and E. Rivalta (2010), A numerical model of dyke propagation in layered elastic media, *Geophys. J. Int.* 180, 1107–1123. http://dx.doi.org/10.1111/j.1365-246X.2009.04495.x.

Malin, M.C., et al. (2007), Context camera investigation on board the Mars Reconnaissance Orbiter, *J. Geophys. Res*. 112, E05S04. http://dx.doi.org/10.1029/2006JE002808.

Massé, M., S. J. Conway, J. Gargani, M. R. Patel, K. Pasquon, A. McEwen, S. Carpy, V. Chevrier, M. R. Balme, L. Ojha, and et al. (2016), Transport processes induced by metastable boiling water under Martian surface conditions, *Nature Geoscience* 9, 425–428. http://dx.doi.org/10.1038/ngeo2706.

Mastin, L. G. (2002), Insights into volcanic conduit flow from an open-source numerical model, *Geochem. Geophys. Geosyst*. 3(7). http://dx.doi.org/10.1029/2001GC000192.

Mazzini, A., and G. Etiope (2017), Mud volcanism: An updated review, *Earth-Science Reviews* 168, 81–112. http://dx.doi.org/10.1016/j.earscirev.2017.03.001.

McCauley, C. A., D. M. White, M. R. Lilly, and D. M. Nyman (2002), A comparison of hydraulic conductivities, permeabilities and infiltration rates in frozen and unfrozen soils, *Cold Reg. Sci. Techno*l. 34(2), 117–125. https://doi.org/10.1016/S0165-232X(01)00064-7.

McEwen, A.S., et al. (2007), Mars Reconnaissance Orbiter's High Resolution Imaging Science Experiment (HiRISE), *J. Geophys. Res.* 112, E05S02. http://dx.doi.org/10.1029/2005JE002605.

Michael, G.G. (2013), Planetary surface dating from crater size–frequency distribution measurements: multiple resurfacing episodes and differential isochron fitting, *Icarus* 226, 885–890. http://dx.doi.org/10.1016/j.icarus.2013.07.004.

Michael, G. G., and G. Neukum (2010), Planetary surface dating from crater size-frequency distribution measurements: partial resurfacing events and statistical age uncertainty, *Earth and Planetary Science Letters* 294, 223–229. http://dx.doi.org/10.1016/j.epsl.2009.12.041.

Michael, G. G., T. Kneissl, and A. Neesemann (2016), Planetary surface dating from crater size–frequency distribution measurements: Poisson timing analysis, *Icarus* 277, 279–285. http://dx.doi.org/10.1016/j.icarus.2016.05.019.

Milana, J. P. (2010), The sieve lobe paradigm: Observations of active deposition, *Geology* 38, 207–210. http://dx.doi.org/10.1130/G30504.1.

Moratto, Z. M., M. J. Broxton, R. A. Beyer, M. Lundy, and K. Husmann (2010), Ames stereo pipeline, NASA's open source automated stereogrammetry software, *41st Lunar and Planetary Science Conference*, Abstract 2364.

Mumma, M. J., G. L. Villanueva, R. E. Novak, T. Hewagame, B. P. Bonev, M. A. DiSanti, A. M. Mandell, and M. D. Smith (2009), Strong release of methane on Mars in northern summer 2003, *Science* 323, 1041–1045. https://doi.org/10.1126/science.1165243.

Oehler, D. Z., and C. C. Allen (2010), Evidence for pervasive mud volcanism in Acidalia Planitia, Mars, *Icarus* 208, 636–657. https://doi.org/10.1016/j.icarus.2010.03.031.

Oehler, D. Z., and C. C. Allen (2012), Giant Polygons and Mounds in the Lowlands of Mars: Signatures of an Ancient Ocean?, *Astrobiology* 12, 601–615. https://doi.org/10.1089/ast.2011.0803.

Oehler, D. Z., and G. Etiope (2017), Methane seepage on Mars: where to look and why, *Astrobiology* 17. https://doi.org/10.1089/ast.2017.1657.

Okubo, C. H. (2016), Morphologic evidence of subsurface sediment mobilization and mud volcanism in Candor and Coprates Chasmata, Valles Marineris, Mars, *Icarus* 269, 23–27, doi:10.1016/j.icarus.2015.12.051.

Orgel, C., E. Hauber, S. van Gasselt, D. Reiss, A. Johnsson, J. D. Ramsdale, and et al. (2018), Gridmapping the Northern Plains of Mars: A New Overview of Recent Water- and Ice-Related Landforms in Acidalia Planitia, *Journal of Geophysical Research: Planets*, 123. https://doi.org/10.1029/2018JE005664.

Parnell, J., A. Mazzini, A., and C. Honghan (2002), Fluid inclusion studies of chemosynthetic carbonates: strategy for seeking life on Mars, *Astrobiology*. 2, 43-57. https://doi.org/10.1089/153110702753621330.

Pfeffer, W., and N. Humphrey (1998), Formation of ice layers by infiltration and refreezing of meltwater, *Annals of Glaciology* 26, 83-91. https://doi.org/10.3189/1998AoG26-1-83-91.

Pondrelli, M., A. P. Rossi, G. G. Ori, S. van Gasselt, D. Praeg, and S. Ceramicola (2011), Mud volcanoes in the geologic record of Mars: The case of Firsoff crater, *Earth and Planetary Science Letters* 304, 511-519. https://doi.org/10.1016/j.epsl.2011.02.027.

R Development Core Team (2011), R: A language and environment for statistical computing. – R Foundation for Statistical Computing, Vienna, Austria. ISBN 3-900051-07-0, URL: http://www.R-project.org/.

Raack, J., S. J. Conway, C. Herny, M. R. Balme, S. Carpy, and M. R. Patel (2017), Water-induced sediment levitation enhances downslope transport on Mars, *Nature Communications* 8, https://doi.org/10.1038/s41467-017-01213-z.

Rice Jr., J. W., and K. S. Edgett (1997), Catastrophic flood sediments in Chryse Basin, Mars, and Quincy Basin, Washington: Application of sandar facies model, J. *Geophys. Res*. 102(E2), 4185–4200. https://doi.org/10.1029/96JE02824.

Rodríguez, J. A. P., K. L. Tanaka, J. S. Kargel, J. M. Dohm, R. Kuzmin, A. G. Fairén, S. Sasaki, G. Komatsu, D.S chulze-Makuch, and Y. Jianguo (2007), Formation and disruption of aquifers in southwestern Chryse Planitia, Mars, *Icarus* 191, 545-567. https://doi.org/10.1016/j.icarus.2007.05.021.

Rubin, D. M., A. G. Fairén, J. Martínez-Frías, J. Frydenvang, O. Gasnault , G. Gelfenbaum, W. Goetz, J. P. Grotzinger, S. Le Mouélic, N. Mangold, H. Newsom, D. Z.Oehler, J. Rapin, J. Schieber, and R. C. Wiens (2017), Fluidized-sediment pipes in Gale crater, Mars, and possible Earth analogs, *Geology* 45 (1), 7–10. https://doi.org/10.1130/G38339.1.

Salvatore, M. R., and P. R. Christensen (2015), On the origin of the Vastitas Borealis Formation in Chryse and Acidalia Planitiae, Mars, *J. Geophys. Res. Planets* 119, 2437–2456. https://doi.org/10.1002/2014JE004682.

Scott, D. H., and K. L. Tanaka (1986), Geologic map of the western equatorial region of Mars., *U.S. Geological Survey Misc. Inv. Series*, Map I-1802.

Skinner, J. A., and A. Mazzini (2009), Martian mud volcanism: Terrestrial analogs and implications for formational scenarios, Mar. Pet. Geol., 26(9), 1866–1878, doi:10.1016/j.marpetgeo.2009.02.006.

Skinner, J. A., and K. L. Tanaka (2007), Evidence for and implications of sedimentary diapirism and mud volcanism in the southern Utopia highland-lowland boundary plain, Mars, *Icarus* 186, 41–59, http://dx.doi.org/10.1016/j.icarus.2006.08.013.

Taisne, B., and C. Jaupart (2009), Dike propagation through layered rocks, *J. Geophys. Res.* 114, B09203. https://doi.org/10.1029/2008JB006228.

Tanaka, K. L. (1997), Sedimentary history and mass flow structures of Chryse and Acidalia Planitiae, Mars, *J. Geophys. Res*. 102(E2), 4131–4149. https://doi.org/10.1029/96JE02862.

Tanaka, K. L. (1999), Debris-flow origin for the Simud/Tiu deposit on Mars, *J. Geophys. Res*. 104(E4), 8637–8652. https://doi.org/10.1029/98JE02552.

Tanaka, K.L., J. A. Skinner Jr., and T. M. Hare (200), Geologic Map of the Northern Plains of Mars, *U.S. Geological Survey Scientific Investigations Map* SIM-2888, Scale 1:15,000,000.

Tran, A., M. L. Rudolph, and M. Manga (2015), Bubble mobility in mud and magmatic volcanoes, *Journal of Volcanology and Geothermal Research* 294, 11-24. https://doi.org/10.1016/j.jvolgeores.2015.02.004.

Turcotte, D. L., and G. Schubert (2002), Geodynamics (2nd ed.), Cambridge University Press.

Vanderkluysen, L., M. R. Burton, A. B. Clarke, H. E. Hartnett, and J. F. Smekens (2014), Composition and flux of explosive gas release at LUSI mud volcano (East Java, Indonesia), *Geochem. Geophys. Geosyst.* 15, 2932–2946. https://doi.org/10.1002/2014GC005275.

Van Rensbergen, P., R. R. Hillis, A. J. Maltman, and C. K. Morley (2003), Subsurface sediment mobilization: introduction, *Geological Society*, London, Special Publications, 216, 1-8. https://doi.org/10.1144/GSL.SP.2003.216.01.01.

Vona, A., G. Giordano, A. A. De Benedetti, R. D'Ambrosio, C. Romano, and M. Manga (2015), Ascent velocity and dynamics of the Fiumicino mud eruption, Rome, Italy, *Geophys. Res. Lett*. 42, 6244–6252. https://doi.org/10.1002/2015GL064571.

Walker, G. P. L. (1989), Gravitational (density) controls on volcanism, magma chambers and intrusions, *Australian Journal of Earth Sciences* 36(2). 149-165. https://doi.org/10.1080/08120098908729479.

Warner, N. H., S. Gupta, F. Calef, P. Grindrod, N. Boll, and K. Goddard (2015), Minimum effective area for high resolution crater counting of Martian terrains, *Icarus* 245, 198-240, https://doi.org/10.1016/j.icarus.2014.09.024.

Webster, C. R., et al. (2018), Background levels of methane in Mars' atmosphere show strong seasonal variations, *Science* 360, 1093-1096. https://doi.org/10.1126/science.aaq0131.

Werner, S. C., A. Ody, and F. Poulet (2014), The source crater of martian shergottite meteorites, *Science* 343, 1343–1346. http://dx.doi.org/10.1126/science.1247282.

Wilson, L., and J. W. Head (1994), Review and analysis of volcanic eruption theory and relationships to observed landforms, *Rev. Geophys*. 32, 221–263. http://dx.doi.org/10.1029/94RG01113.

Wilson, L., and J. W. Head (2004), Evidence for a massive phreatomagmatic eruption in the initial stages of formation of the Mangala Valles outflow channel, Mars, *Geophys. Res. Lett*. 31, L15701. https://doi.org/10.1029/2004GL020322.

Wilson, L., and J. W. Head (2017), Eruption of magmatic foams on the Moon: Formation in the waning stages of dike emplacement events as an explanation of "irregular mare patches", *Journal of Volcanology and Geothermal Research* 335, 113–127. https://doi.org/10.1016/j.jvolgeores.2017.02.009.

Wilson, L., and P. J. Mouginis-Mark (2014), Dynamics of a fluid flow on Mars: Lava or mud?, *Icarus* 233, 268-280, doi:10.1016/j.icarus.2014.01.041.

Withjack, M. O., and C. Scheiner (1982), Fault patterns associated with domes--an experimental and analytical study, *AAPG Bulletin* 66, 302-316. https://doi.org/10.1306/03B59AFD-16D1-11D7-8645000102C1865D.

Yin, H., and R. H. Groshong (2007), A three-dimensional kinematic model for the deformation above an active diaper, *AAPG Bulletin* 91, 343–363. https://doi.org/10.1306/10240606034.

8. Acknowledgment

We appreciate the efforts of the instrument teams (MOLA, HRSC, CTX, HiRISE) who acquired and archived the data used in our investigation. P.B. is thankful to Gregory Michael for the help with the crater counting and Peter Fawdon for the help with the HiRISE DEMs production. We are thankful to Adriano Mazzini, James Skinner and an anonymous reviewer for their constructive comments and inspiring suggestions which significantly improve this manuscript and to David Baratoux for handling the associated editorial process. Part of this research (V.Š.) was supported by Center for Geosphere Dynamics (UNCE/SCI/006). The shapefiles with the position of studied features and shapefiles associated with the crater counting are available for download at https://doi.org/10.5281/zenodo.2536019.

9. Figures

Figure 1: Regional map of the southern part of Chryse Planitia at the terminations of the large outflow channels of Ares, Simud, and Tiu Valles in which material was transported from south to north. The differently colored dots show the position of studied landforms. Yellow symbols: Type 1 (cones); blue:

Type 2 (pie-like features); white: Type 3 (domes); violet: Type 4 (irregular sheet-like features); red: Type 5 (large flow-like features). The white solid polygon encloses the area used for determination of crater model age. The blue polygons associated with impact craters denote the presence of rampart ejecta and its extension. The images is based on a HRSC DEM basemap.

Figure 2: Examples of five types of studied landforms interpreted as the surface manifestations of subsurface sediment mobilization. In all panels north is up. (a) Type 1, cones; (image: HiRISE ESP_022025_2000, centered 19.73°N, 322.44°E); (b) Type 2, pies (image: CTX G17_024926_1992_XI_19N038W, centered 18.73°N, 321.74°E); (c) Type 3, domes (HiRISE ESP_021748_1990, centered 18.86°N, 322.63°E); (d) Type 4, irregular pies (CTX P17_007692_1956_XN_15N040W, centered 14.24°N, 319.76°E). The white dashed line marks the perimeter of the feature, (e) Type 5, channelized flow-like features (CTX P17_007639_1997_XN_19N034W, centered 19.85°N, 326.02°E). Types 1-3 were already described by *Komatsu et al*. [2016].

Figure 3: Image showing an example of feature of Type 5. (a) Features of this class are displaying a flow-like appearance commonly associated with central channels and levees. (b) The schematic drawing shows by dark grey color the spatial distribution of the material associated with this flow-like feature. Marked are also features of other types and cluster of secondary craters associated with the Mojave impact. Detail of the central pond-like depression (c) from which multiple channels originate (d). The white arrow marks the position of the inner channel. (e) A highly sinuous channel (marked by white arrow) can be identified in the part of the flow where deposition prevails. The image is based on the mosaic of CTX images P15_007059_1995_XN_19N036W and B19_016856_1990_XI_19N035W, centered 19.38°N, 323.89°E.

Figure 4: An example of cone-like feature of Type 3 with close up detail of the summit area. (a) Detail of cone-like feature with marked position of topographic measurement based on HiRISE DEM. The cone has a well-developed central summit area with a small knob in the canter (HiRISE image ESP_025137_1995, centered 19.04°N, 322.64°E). (b) Detail of the knob which is characterized by

irregular shape and relatively steep flanks. (c) Topographic profile reveals that the cone is around 90 meters high and that the central knob is within the range of several meters.

Figure 5: Charts showing dependencies in the spatial distribution of all studied edifices and in the average distances between features of Type 2. (a) The spatial distribution of studied features show that edifices of different types occur preferentially in specific latitudes, however, the area of their extension often overlaps with areas of other types. (b) The nearest neighbor distance calculated for features of Type 2 plotted versus the feature size of the same objects revealed that features of Type 2 have a strong tendency for non-overlapping each other.

Figure 6: Crater model ages derived from crater count analysis of Area 1 marked on the Figure 1. Relative likelihood functions inset. The differential crater size–frequency curve indicates crater model ages of $\mu 880^{+0.2}_{-0.2}$ Ma, $\mu 1.7^{+0.2}_{-0.2}$ Ga, $\mu 3.2^{+0.2}_{-0.5}$ Ga, and $\mu 3.2^{+0.3}_{-0.8}$ Ga, respectively. This suggests that the unit experienced several resurfacing events which were able to remodel the surface. The studied features therefore have to be younger than those resurfacing events. It should be also noted that as the crater population above 7 km is consistent in age with that from 2-7 km, this may be the age of an underlying surface. μ is a function representing the uncertainty of calibration of the chronology model [*Michael et al*., 2016].

Figure 7: Alternative scenarios for the formation of the investigated landforms in southern Chryse Planitia. The topography is derived from a regional HRSC DEM, the subsurface structures are all inferred and not to scale. (a) Igneous volcanism. If magma rises from crustal magma chambers trough dikes, it would be likely that volcanic landforms were not only emplaced in lowlands, but also on highlands. Inset 1 (modified from [*Gaffney and Damjanak*, 2006]) shows a mechanism which would tend to localize volcanism in lowlands, but it would requires dikes to cut the transition from lowlands to highlands. Inset 2 shows hydrovolcanic activity that would be expected if groundwater or -ice would have been present during magma ascent (as indicated by rampart craters). (b) Sedimentary volcanism. The location of the investigated landforms exclusively in the lowlands (Fig. 1) suggests a genetic link to sediments (shown in bluish tones). It is not clear from which depth(s) the mobilized sediment comes

from, and any of the depicted scenarios may apply. Insets 3 and 4 show different possibilities for the ascent off liquefied sediment and were derived from *Mazzini and Etiope* [2017] and *Skinner and Mazzini* [2009], respectively. They show that sediment from several strata in the stratigraphy may have contributed to the extrusions, consistent with the complex stratigraphy in Chryse Planitia [*Jones et al*., 2016].

Figure 8: The schematic drawing shows how the variations in the effusion rates and viscosities could lead to the formation of features of different types.

Table 1: Frequencies of the studied edifices, Nearest neighbor ratios, and circularities.

Figure 1.

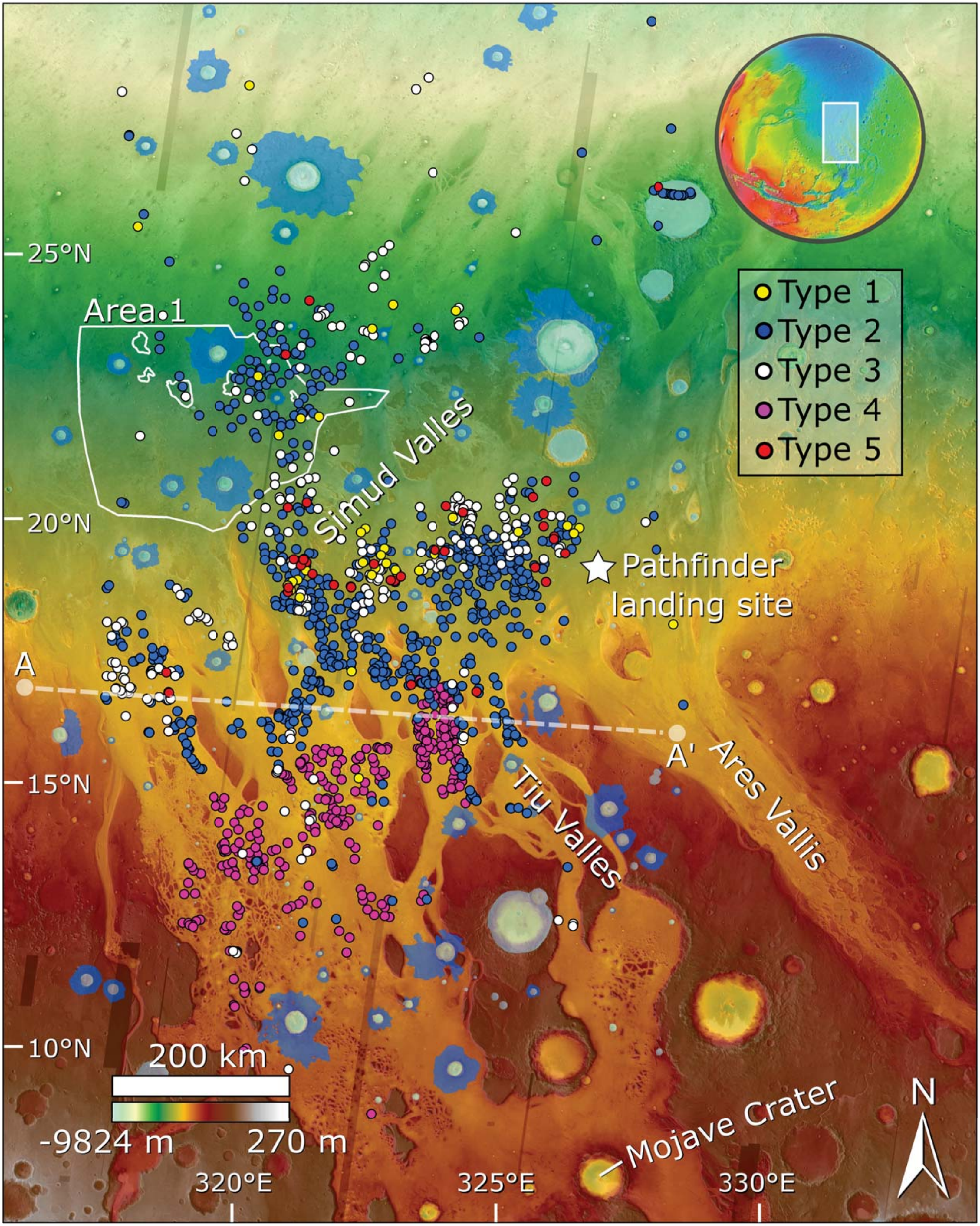

Type 1
Type 2
Type 3
Type 4
Type 5
Area 1
Simud Valles
Pathfinder landing site
Tiu Valles
Ares Vallis
Mojave Crater
A
A'
25°N
20°N
15°N
10°N
320°E
325°E
330°E
200 km
-9824 m
270 m
N

Figure 2.

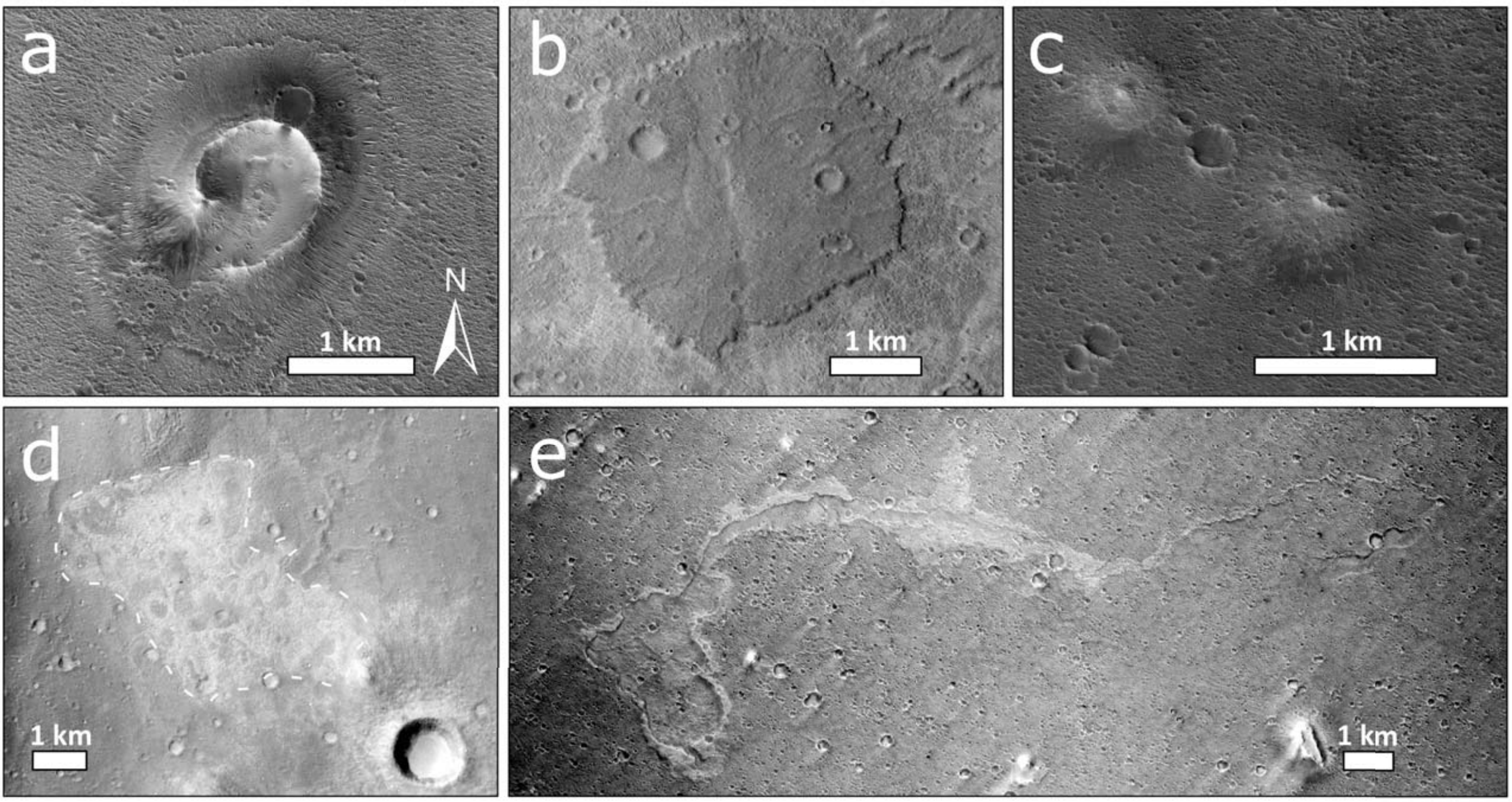
a
N
1 km
b
1 km
c
1 km
d
1 km
e
1 km

Figure 3.

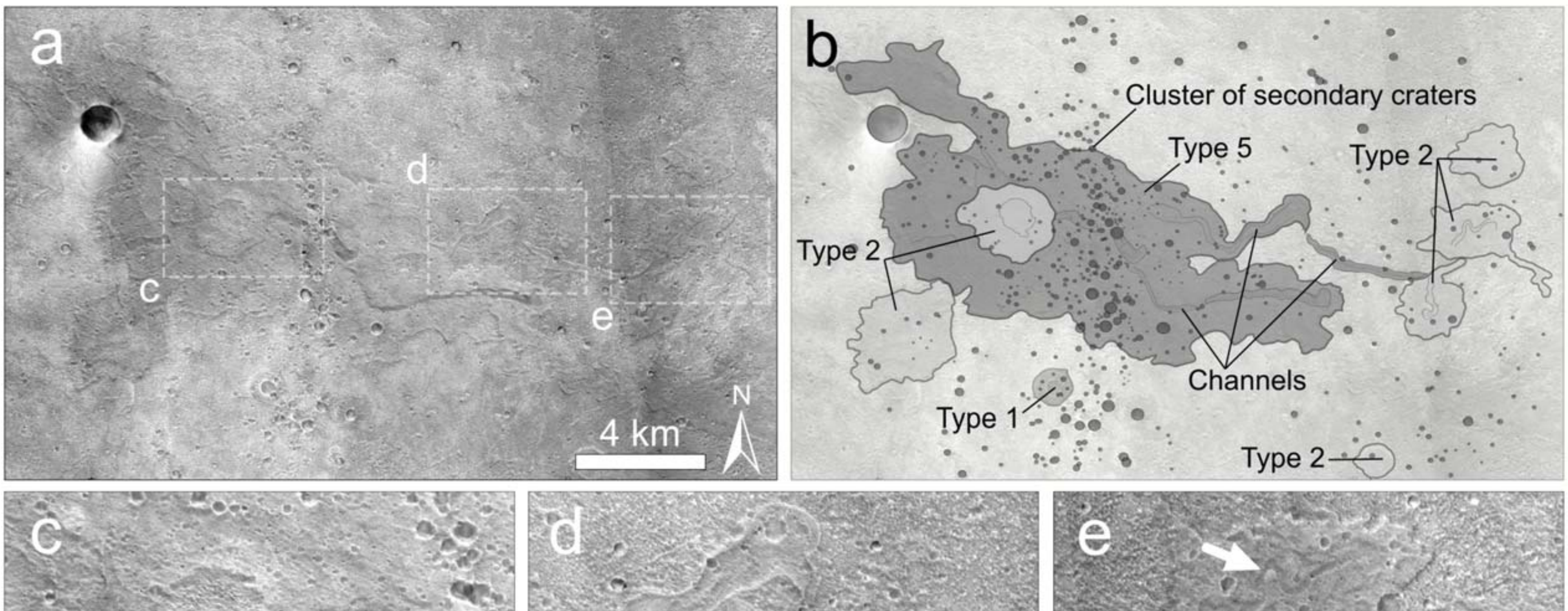

a
c
d
e
4 km
N
b
Cluster of secondary craters
Type 5
Type 2
Type 2
Channels
Type 1
Type 2
c
d
e

Figure 4.

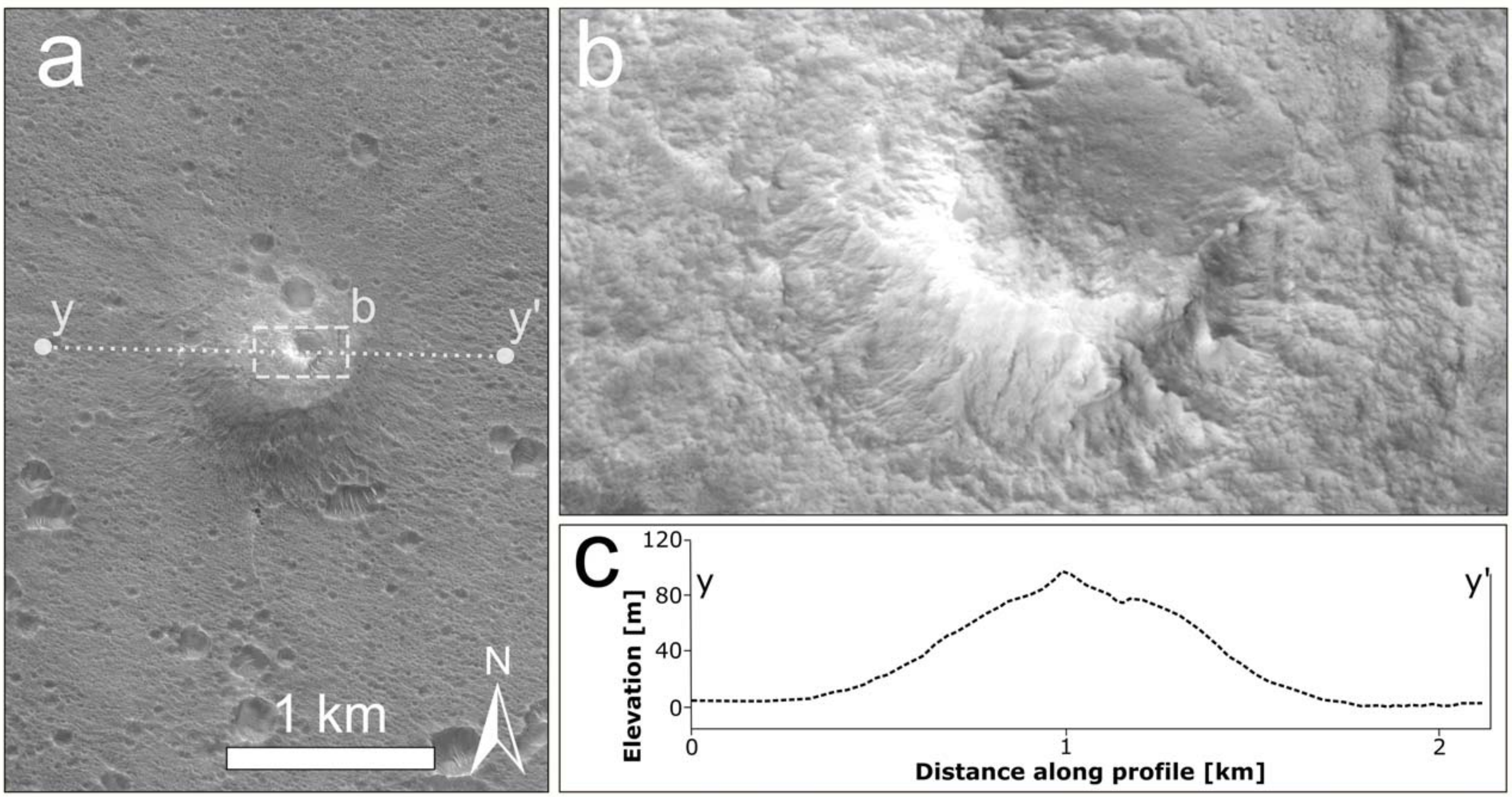

a
y
b
y'
1 km
N
b
C
y
y'
120
80
40
0
Elevation [m]
0
1
2
Distance along profile [km]

Figure 5.

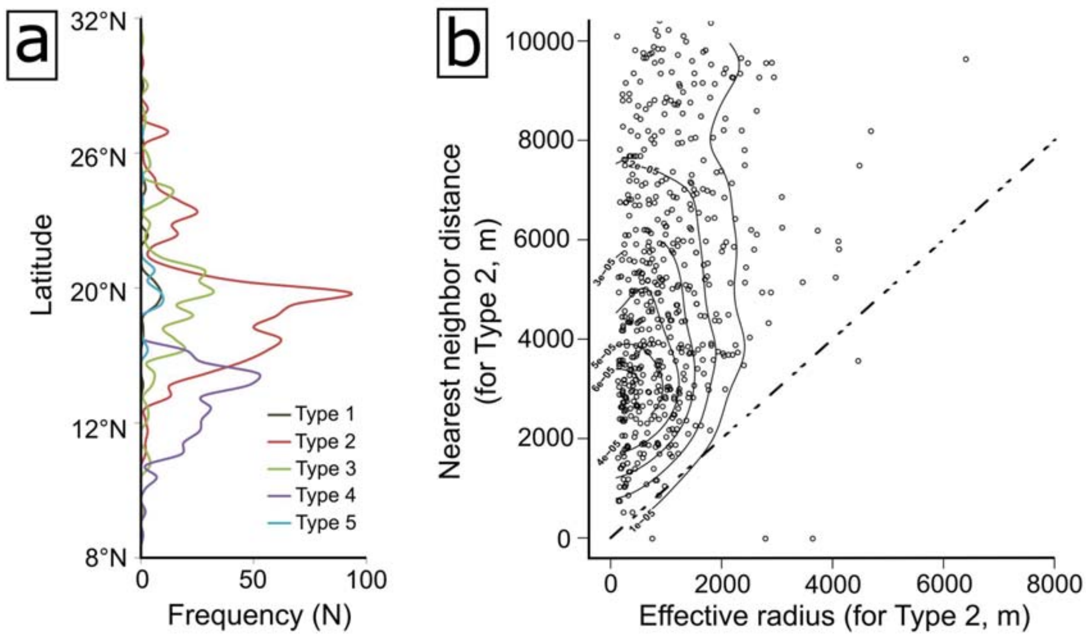
a
32°N
26°N
20°N
12°N
8°N
Latitude
0
50
100
Frequency (N)
Type 1
Type 2
Type 3
Type 4
Type 5
b
10000
8000
6000
4000
2000
0
Nearest neighbor distance
(for Type 2, m)
0
2000
4000
6000
8000
Effective radius (for Type 2, m)

Figure 6.

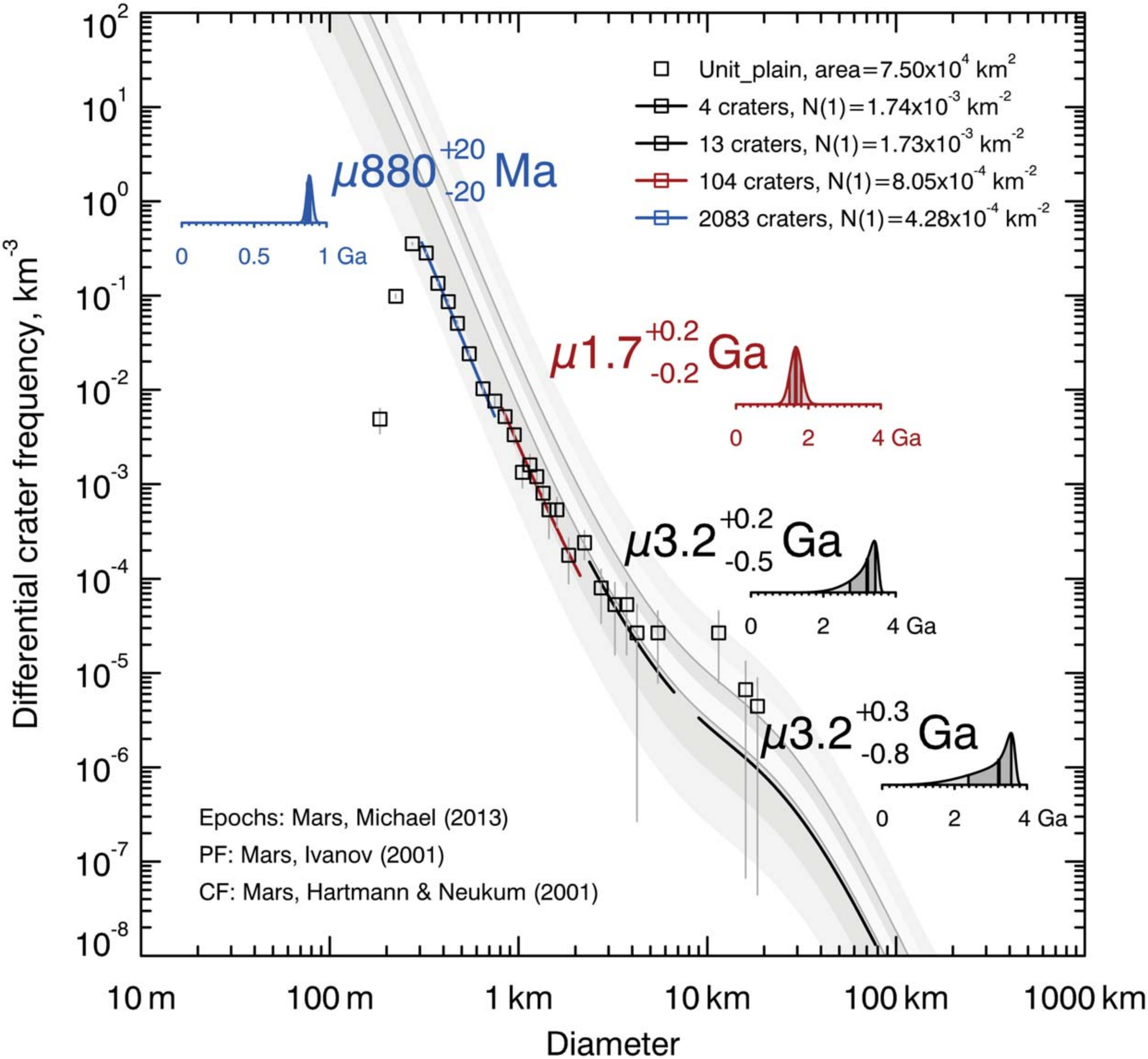

Unit_plain, area=7.50x10^4 km^2
4 craters, N(1)=1.74x10^-3 km^-2
13 craters, N(1)=1.73x10^-3 km^-2
104 craters, N(1)=8.05x10^-4 km^-2
2083 craters, N(1)=4.28x10^-4 km^-2
μ880 +20 -20 Ma
0 0.5 1 Ga
μ1.7 +0.2 -0.2 Ga
0 2 4 Ga
μ3.2 +0.2 -0.5 Ga
0 2 4 Ga
μ3.2 +0.3 -0.8 Ga
0 2 4 Ga
Epochs: Mars, Michael (2013)
PF: Mars, Ivanov (2001)
CF: Mars, Hartmann & Neukum (2001)
Differential crater frequency, km^-3
Diameter
10 m
100 m
1 km
10 km
100 km
1000 km
10^2
10^1
10^0
10^-1
10^-2
10^-3
10^-4
10^-5
10^-6
10^-7
10^-8

Figure 7.

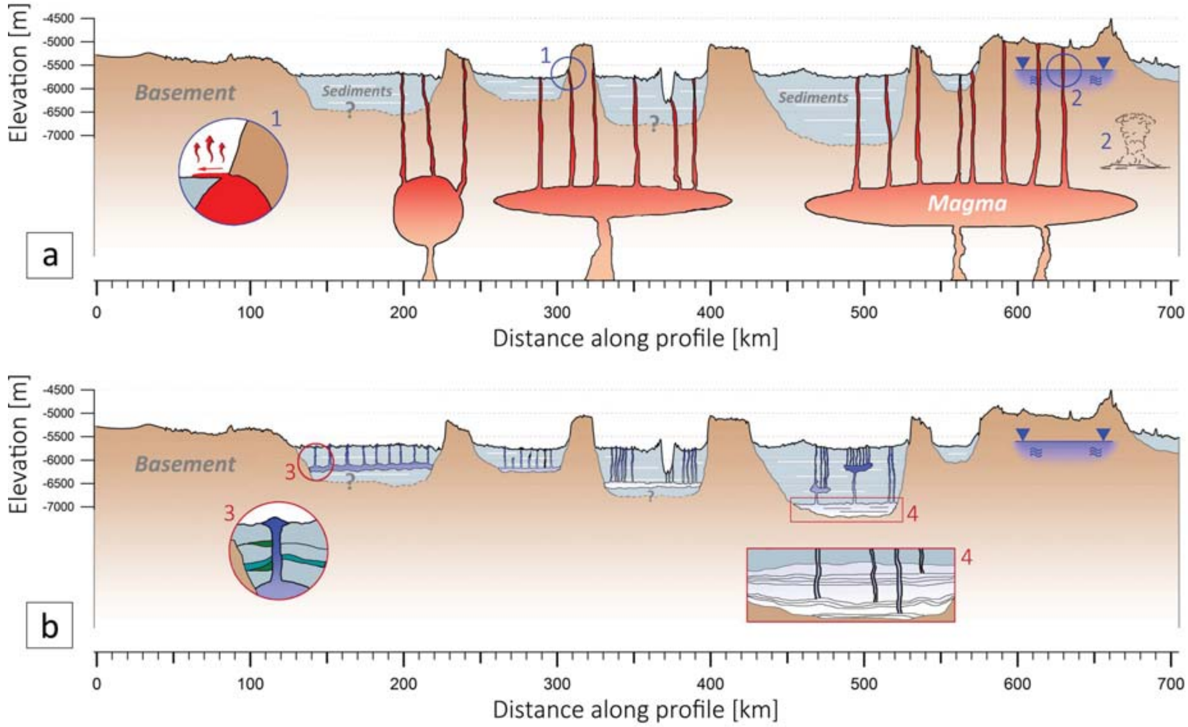
Elevation [m]
-4500
-5000
-5500
-6000
-6500
-7000
Basement
Sediments
Sediments
Magma
1
2
a
0
100
200
300
400
500
600
700
Distance along profile [km]
Elevation [m]
Basement
3
4
b
Distance along profile [km]

Figure 8.

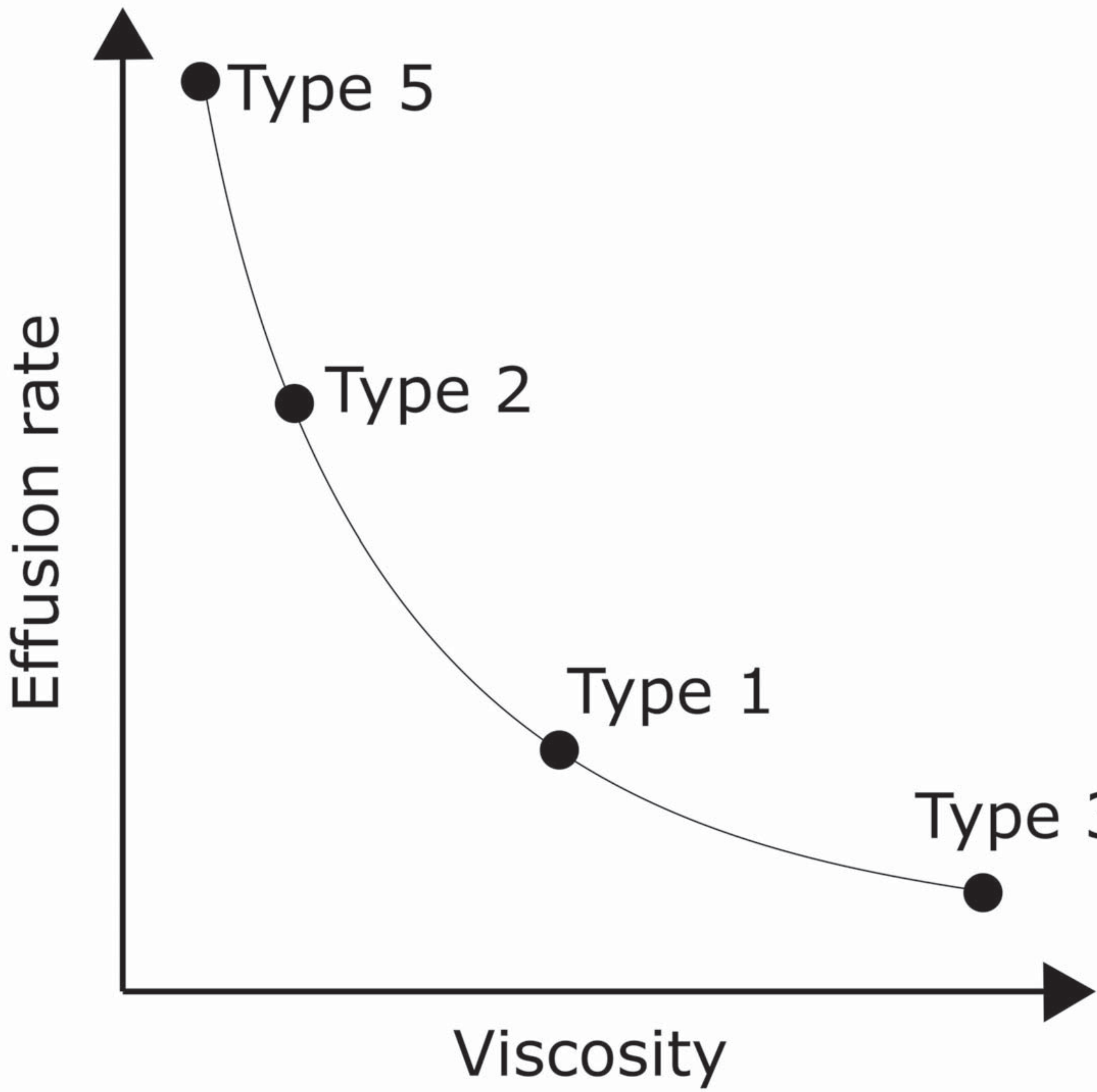
Type 5
Type 2
Type 1
Type 3
Effusion rate
Viscosity

	Frequency (N)	Frequency (%)	Nearest neighbor ratio	Circularity (mean)
Type 1	36	2.7	0.84	0.85
Type 2	679	51.5	0.51	0.8
Type 3	259	19.7	0.44	0.85
Type 4	309	23.4	0.57	0.7
Type 5	35	2.7	0.69	N/A
All features	1318	100.0	0.53	N/A

Table 1: Frequencies of the studied edifices, Nearest neighbor ratios and circularities.